2D Nanostructures

International Edition: DOI: 10.1002/anie.201912247
German Edition: DOI: 10.1002/ange.201912247

Snapshots of Dynamic Adaptation: Two-Dimensional Molecular Architectonics with Linear Bis-Hydroxamic Acid Modules

Chao Jing[+], Bodong Zhang[+], Sabine Synkule, Maryam Ebrahimi, Alexander Riss, Willi Auwärter, Li Jiang, Guillaume Médard, Joachim Reichert, Johannes V. Barth,* and Anthoula C. Papageorgiou**

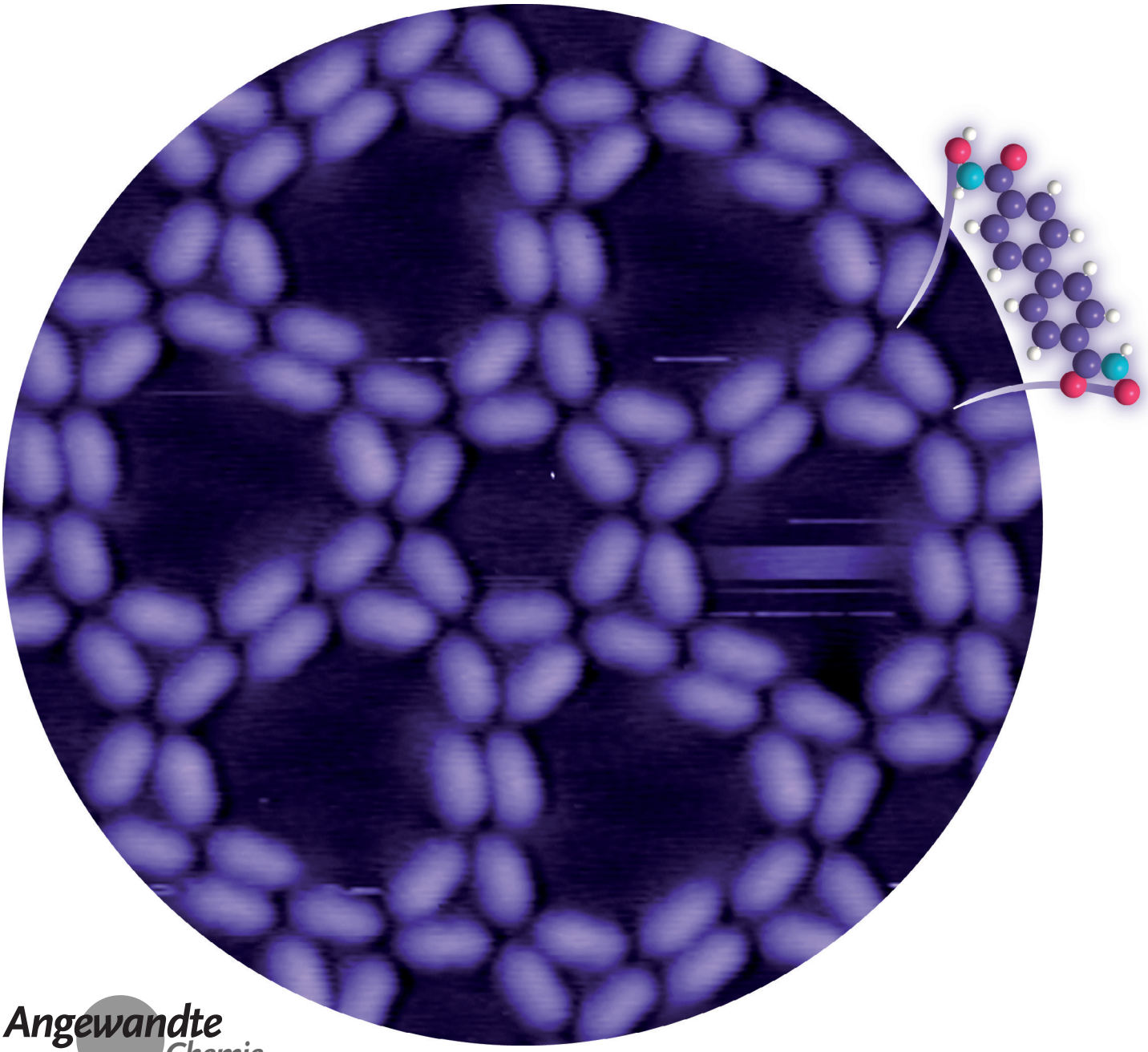

Abstract: *Linear modules equipped with two terminal hydroxamic acid groups act as the building block of diverse two-dimensional supramolecular motifs and patterns with room-temperature stability on the close-packed single-crystal surfaces of silver and gold, revealing a complex self-assembly scenario. By combining multiple investigation techniques (scanning tunneling microscopy, atomic force microscopy, X-ray photoelectron spectroscopy, and density functional theory calculations), we analyze the characteristics of the ordered assemblies which range from close-packed structures to polyporous networks featuring an exceptionally extended primitive unit cell with a side length exceeding 7 nm. The polyporous network shows potential for hosting and promoting the formation of chiral supramolecules, whereas a transition from 1D chiral randomness to an ordered racemate is discovered in a different porous phase. We correlate the observed structural changes to the adaptivity of the building block and surface-induced changes in the chemical state of the hydroxamic acid functional group.*

Introduction

In the past decades, the miniaturization and molecular-level control of materials have witnessed a plethora of mathematically described tessellations achieved via atomically precise materials engineering. In this context, the realization of two-dimensional (2D) nanostructures is attracting increasing attention.[1] 2D supramolecular structures are expected to have promising applications in molecular devices and nanochips.[2] In particular, the modular assembly of intricate structures and the associated design principles are posing a current challenge in this area. Recent breakthroughs include the concept of self-similarity expressed in intermolecular interactions, which lead to fractal structures[3] and high-order supramolecular networks.[4] Additionally, the use of the extended coordination sphere of certain metal atoms, such as lanthanides, enabled the construction of Archimedean tessellations and 2D quasicrystals by the formation of well-defined nodes.[5]

Here we introduce a bioinspired building block, hydroxamic acid, for the construction of sophisticated, functional, and tunable 2D architectures. Hydroxamic acids are ubiquitous in nature and widely applied in chemistry, chemical biology, and medicine.[6] More recently, they have shown promise in dye-sensitized solar cells as anchor groups optimizing the adsorption of dyes and the power-conversion efficiency.[7] The hydroxamic acid functional units are suitable binding groups for 2D self-assembled structures, with a bonding strength on the native oxides of metal surfaces determined to lie between carboxylic acid and thiol groups;[8] however, they are hitherto unexplored in the context of directing in-plane 2D structures. Notably, hydroxamic acids bear a great versatility for intermolecular interactions and are predicted to form 25 possible two-fold bonding nodes based on hydrogen bonding.[9]

Inspired by previous work on tectons containing multiple head groups, which enable the formation of intricate 2D tessellations, we designed and synthesized a symmetric linker molecule with opposing hydroxamic acid head groups and a biphenyl backbone as an "inert" and tuneable moiety (biphenyl-4,4′-dihydroxamic acid, BPDH, Figure 1 A). We report on the adsorption of this tecton and its dynamic

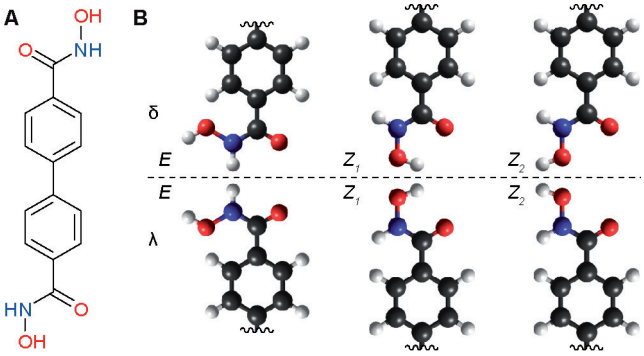

Figure 1. Biphenyl-4,4′-dihydroxamic acid (BPDH). A) Structural formula. B) Six possible surface-confined forms of a phenyl hydroxamic acid moiety relevant for node formation. C, O, N, and H atoms are shown in black, red, blue, and white, respectively. *E*- and *Z*-isomers are the result of C–N bond rotation (left and middle panels); the possible rotation around the N–O bond of a *Z*-isomer results in two rotamers differing in the positions of the hydroxyl H (middle and right panels); confinement of the hydroxamic acid C atom on a surface results in a chiral center which gives rise to the δ and λ surface enantiomers (top vs. bottom panels).

[*] Dr. C. Jing,[+] Dr. B. Zhang,[+] S. Synkule, Dr. M. Ebrahimi, Dr. A. Riss, Prof. Dr. W. Auwärter, Dr. L. Jiang, Dr. J. Reichert, Prof. Dr. J. V. Barth, Dr. A. C. Papageorgiou
Physics Department E20, Technical University of Munich
James Franck Straße 1, 85748 Garching (Germany)
E-mail: joachim.reichert@tum.de
jvb@tum.de
a.c.papageorgiou@tum.de
Dr. C. Jing[+]
Key Laboratory for Advanced Materials, School of Chemistry and Molecular Engineering, East China University of Science and Technology
Shanghai, 200237 (P. R. China)
Dr. M. Ebrahimi
Department of Chemistry, Lakehead University
955 Oliver Rd, Thunder Bay, ON P7B 5E1 (Canada)
Dr. G. Médard
Chair of Proteomics and Bioanalytics, Technical University of Munich
Emil Erlenmeyer Forum 5, 85354 Freising (Germany)
[+] These authors contributed equally to this work.

Supporting information and the ORCID identification number(s) for the author(s) of this article can be found under: https://doi.org/10.1002/anie.201912247.

adaptation into intricate self-assembled structures featuring chiral pores. To this end, we employ an integrated characterisation approach at the atomic scale encompassing scanning tunnelling microscopy (STM) and non-contact atomic force microscopy (nc-AFM) complemented with X-ray photoelectron spectroscopy (XPS) and density functional theory (DFT) calculations.

Results and Discussion

We have created films of submonolayer coverage of BPDH molecules on Au(111) and Ag(111) surfaces. To characterize these, we will first address the adsorption of the isolated molecules on the surface. Subsequently, we will focus on the supramolecular self-assembly. Experimental and computational methods are detailed in the Supporting Information.

Isolated Molecule

BPDH molecules might exhibit a plethora of isomers, including *Z*–*E*, referring to a single hydroxamic acid group (Figure 1B), *cis*–*trans*, referring to the relative configuration of the two hydroxamic acid groups in a single molecule, *amide*–*iminol* tautomers (Figure S1, Supporting Information), and zwitterionic forms.[10] The scanning probe microscopy study reveals very similar topographies for a single isolated molecule of BPDH on both surfaces (Figures 2A–C and S2). Under STM, they are visible as bright rods, consistent with the biphenyl backbone lying parallel to the Ag substrate along the $\langle 1\bar{2}1\rangle$ set of surface directions. In nc-AFM (Figure 2C), the biphenyl moiety appears relatively flat as can be seen from the small variation of brightness across the backbone of the molecule.[11] Regrettably, the end groups proved to be elusive.[12] In agreement with experimental data, AFM simulations reveal little contrast from the functional group (Figure S3). According to our DFT simulation, BPDH is more stable in the *Z*-isomer amide form in the gas phase (Figure S1). Moreover, the existence of the iminol or zwitterionic form on the surface is not supported by the respective XPS data (see below). Hence, to identify the preferential configuration of BPDH on Ag(111), the *cis*- and *trans*-isomers in the *Z*-type amide terminal groups as well as the hydroxamate forms were considered for simulating the single BPDH molecule adsorbed on Ag(111) (Figure S3). The DFT simulations show that the biphenyl dihedral angle is reduced from 38° for the gas phase molecule to ≈15° when adsorbed on the surface. From these, only the *trans*-amide form matched the biphenyl axis alignment along the $\langle 1\bar{2}1\rangle$ set of surface directions observed under STM (Figure 2D). The *cis*-amide form deviates by 9° from the observed alignment and is less favored by 0.05 eV. Furthermore, for both *trans*- and *cis*-BPDH with dissociated O–H bonds, the biphenyl moiety is predicted to align along the $\langle 2\bar{3}1\rangle$ set of directions on the Ag surface, in contrast to experimental observations.

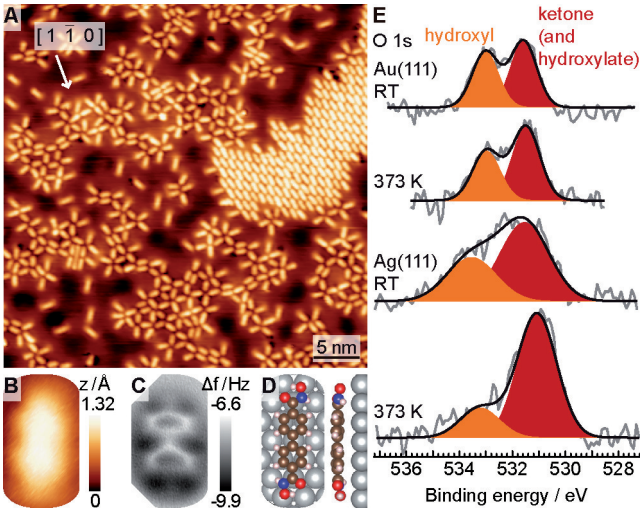

Figure 2. A) STM overview topography of BPDH on Ag(111) following RT deposition (5 K, $V_s = 1.00$ V, $I = 0.01$ nA). The white arrow indicates the Ag [1$\bar{1}$0] direction. B)–D) Images of isolated BPDH on Ag(111) at the same scale: B) STM topography (5 K, $V_s = 0.10$ V, $I = 0.02$ nA); C) nc-AFM frequency shift (tip–sample distance decreased by 10 pm with respect to the STM set point above the silver surface); D) top view and side view of the DFT-optimized structure (C, O, N, H, and Ag atoms are represented in brown, red, blue, white, and silver color, respectively). E) O 1s spectra of BPDH molecules adsorbed at RT and post-annealed at 373 K on both Au(111) and Ag(111). The background-subtracted experimental data (gray lines) are fitted (black lines) with two components for hydroxyl (in orange) and ketone plus hydroxylate (in red) contributions.

Chemical State of Molecular Ensembles

The O 1s spectra of BPDH molecules on the Au(111) and Ag(111) surfaces after room-temperature (RT) deposition (Figure 2E) provided a signature of the chemical state of the functional group. On Au(111), two peaks at 531.6 eV and 533.0 eV with approximately 1:1 ratio can be assigned to the almost equal presence of C=O and –OH groups, respectively. The corresponding N 1s signal appears as a single peak at 399.3 eV (Figure S4). For BPDH adsorbed on Ag(111) at RT, there is a change in the ratio of the components of the O 1s signal, with the high-energy component attributed to the –OH group being partially depleted. This effect is accentuated after annealing to ≈373 K (Figure 2E). This is consistent with a gradual deprotonation of the –OH group commencing already at RT.[13] Discrepancies between the peaks of BPDH molecules on Ag(111) and Au(111) are tentatively ascribed to differences in the adsorption geometry, which is affected by supramolecular interactions (addressed in the subsequent sections). On silver, the N 1s signal displays a peak at 399.4 eV (Figure S4). We therefore infer that after RT deposition, the hydroxamic acid moieties are mostly intact on both surfaces, whereas annealing is promoting the surface-induced cleavage of the O–H bond, an effect which is more pronounced on Ag(111).

Close-Packed Structures

Close-packed structures appear already at submonolayer BPDH coverages and dominate the STM images at higher coverages on both Ag(111) (Figures 2A and 3A) and Au(111) (Figure S2A). The molecules form 1D hydrogen-bonded chains which aggregate and result in 2D islands, reminiscent of the assembly of related biphenyl-4,4′-dicarboxylic acid on Au(111) and Cu(111).[14] Close inspection reveals that the molecular rods appear asymmetric in the STM image with one end being brighter than the other. Interestingly, the direction of the bright ends (marked with yellow and black rectangles in Figure 3A) inverses between neighboring chains resulting in a regular structure with a molecular density of 1.0 molecule nm^{-2}. Since the same supramolecular structure was identified on both Ag(111) and Au(111), we modelled it with intact molecules on Ag(111)—in accordance with the XPS signals (Figure 2E)—in the favourable *trans*-conformation (Figure S5). The STM image agrees well with the partially overlaid DFT model (Figure 3A). Each hydroxamic acid group participates in two hydrogen bonds (−OH···O=C−) with its neighbor, which further stabilize the molecule in the close-packed structure (adsorption energy of −2.4 eV) compared to the isolated molecular adsorbate (−2.1 eV).

The interaction between adjacent molecules is similar to the packing of carboxylic acids on planar metal surfaces.[14] The amino group does not seem to direct the assembly. We note that more recent reports on the self-assembly of dicarboxylic-acid-containing molecules indicate that the corresponding overlayer unit cell can also be expressed after (partial) dissociation of the O–H bond,[14d,15] an event which cannot be excluded based on our XPS data, especially on the Ag(111) surface.

Superimposing the simulated structure on the STM data, we find that the brighter ends coincide with the protruding functional group (see Figure 3). Nc-AFM data of close-packed molecular arrangements on both Ag and Au surfaces reveal different tilt angles of the phenyl rings with respect to the surface plane, evidenced by the variation of intensity in the frequency shift (Figure S6). The DFT simulation reproduces the tilt variations of the phenyl rings on the silver surface with dihedral angles of 6° and 22°, showing an unexpected effect of the molecule–molecule interaction on the molecular conformation. Some defects in the packing, such as a broken sequence of the bright/dark visualization of the molecular end groups, are indicated by ellipses in Figure 3A. In other areas, small deviations of the direction of the molecular modules can be observed (Figure 2A). These are signs of the simultaneous expression of different hydrogen-bonding schemes, presumably further facilitated by molecular-bond rotations and conformational adaptability. This diversity of hydrogen-bonded building motifs is characteristic of biological modules and can result in many 2D supramolecular assemblies with very similar lattice vectors.[16] Additionally, the surface or tunneling may mediate isomerizations,[17] such as between the Z_1- and Z_2-isomers (Figure 1B), without the need of bond rotations.

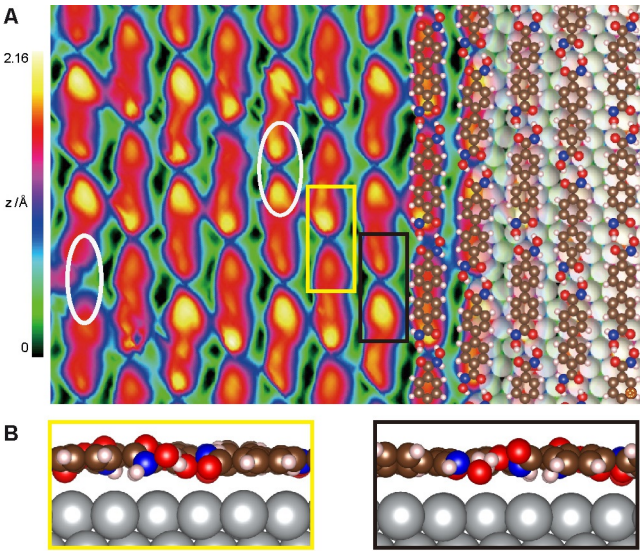

Figure 3. Close-packed structure of BPDH molecules on the Ag(111) substrate. A) STM image in a false-color scale (5 K, $V_s = 1.00$ V, $I = 0.01$ nA) merged with a top view of the simulated structure. B) Side views of simulated bonding nodes indicated by the corresponding rectangles in the STM image. C, O, N, H, and Ag atoms are represented in brown, red, blue, white, and silver color, respectively.

Additionally, the molecules arrange in different types of molecular clusters with node motifs forming vertices between 2, 3, 4, or 5 molecules (Figure 2A), which demonstrates the structural flexibility of the employed functional group in node construction. It should be emphasized that here, we use the terms "node" and "vertex" to describe the proximity of 2 or more functional groups although the molecular axes (lines passing through the biphenyl backbone) do not necessarily all intersect at the same point (examples are illustrated in Figure S7). Such nodes were also observed on Au(111), where the molecular structures formed assemblies that were confined to the fcc domains (Figure S2B).

Polyporous Network

Notably, an intricate, highly ordered tiling was observed solely on Ag(111) (Figure 4), reminiscent of a sliced lemon. It appears on surfaces investigated at RT with submonolayer coverages and coexists with less ordered molecular clusters and the cross-phase described in the next section. It extends in domains with dimensions of more than 50 nm across (Figure S8) and is characterized by an unusually extended hexagonal lattice of p6 symmetry oriented along the high symmetry axes of the substrate (Figure 4A), described by the epitaxial matrix $\begin{pmatrix} 25 & 0 \\ 0 & 25 \end{pmatrix}$. The unit cell (outlined in white in Figure 4A) encompasses 24 molecules in a relatively low molecular density of 0.53 molecule nm^{-2} (approximately half of the densely packed phase). The large unit cell of this structure impedes DFT simulations, however, we will describe the observed network geometry and propose a tentative molecular model hereafter.

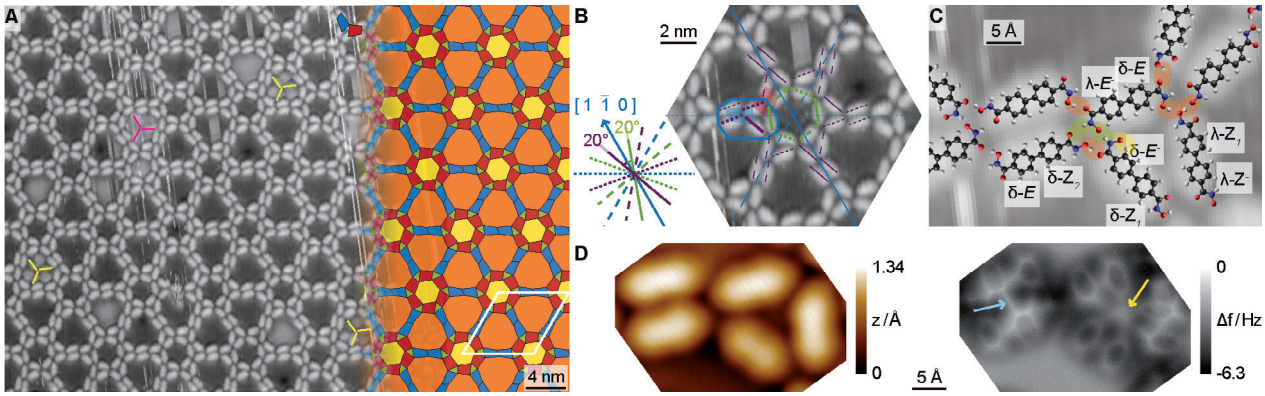

Figure 4. Polyporous network of BPDH molecules on Ag(111). A) STM image (298 K, $V_s = 0.91$ V, $I = 0.09$ nA) partially overlaid with the colored tessellation on the right side of the image. The unit cell is shown in white on the tessellation area. B) Detail of the STM structure overlaid with green and purple lines indicating the molecular axes. Solid lines and different dotted lines of the same color correspond to the same substrate direction and its rotation by 120° and 240°. High-symmetry axes of the Ag substrate shown in blue, molecular-axes orientations shown in green and purple. C) Tentative molecular model overlaid on the STM image. C, O, N, and H atoms are shown in black, red, blue, and white, respectively. D) STM topography (left, 5 K, $V_s = 0.10$ V, $I = 0.02$ nA) and corresponding nc-AFM frequency shift (tip–sample distance decreased by 95 pm with respect to a set point above the silver surface) of the fragment of the network corresponding to the blue tile outlined in (B).

This complex structure comprises two distinct supramolecular motifs. These inequivalent vertices of four molecules span the complete pattern by operations of 60° rotations (permitted by the sixfold symmetry of the Ag substrate surface layer) and translation dictated by the unit cell. The red and blue tiles in Figure 4A correspond to these two vertices by linking the (approximate) centers of the related biphenyl moieties. Thus, the network can be described by a tiling consisting of two building blocks corresponding to the nodes of the molecules (red and blue tiles) and three building blocks corresponding to the voids (orange, yellow, and green tiles). The pores differ significantly in size, with the orange, yellow, and green pores (see Figure 5) having areas of ≈9.3, 4.2 and 0.5 nm^2, respectively, based on the van-der-Waals radii of the atoms in the proposed model. The smaller pores could potentially stabilize a small molecule or atomic adsorbate(s). Indeed, this seems to be the case in the AFM image of a similar pore shown in Figure 4D (yellow arrow): the cavity has a small round protrusion in its center, the appearance of which is consistent with the dimensions of a single-atomic or small molecular species such as an Ag adatom or CO molecule.

A careful examination of the repeated pattern in Figure 4B reveals that all BPDH molecules in this structure have their biphenyl axis aligned with respect to the Ag(111) high-symmetry direction at ≈±20°. The −20° clockwise rotation of the BPDH molecules enclosing the yellow-marked pore in Figure 4A,B and the +20° anti-clockwise rotation of the molecules around the orange-marked pore result in a gyrated tiling with organizational chirality.[18] The two enantiomeric domains (labelled *R* and *S*) are displayed side by side in Figure 5A,B. The chirality of the network is transferred to its pores and is expected to be crucial in directing host–guest interactions.[19]

The confinement of guest molecules manifests in the data of Figure 4A. The larger pores (yellow and orange) do not appear with uniform contrast. The streaking observed occasionally within them is evidence of mobile molecules. Importantly, within some of the pores substructures appear that are reminiscent of propellers. These correspond to the time-averaged positions of the guest molecules during the

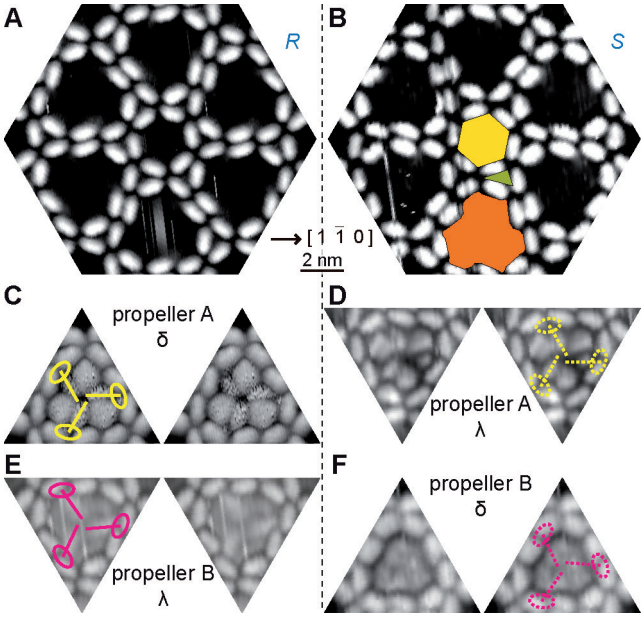

Figure 5. Organizational chirality in a polyporous network of BPDH molecules on Ag(111) and enantiomeric interactions of supramolecularly assembled guests. A) STM image of an *R* domain motif (298 K, $V_s = 0.91$ V, $I = 0.10$ nA). B) STM image of an *S* domain motif (298 K, $V_s = 1.44$ V, $I = 0.10$ nA) overlaid with colored blocks (orange, yellow, and green) corresponding to the areas assigned to the different pores (≈9.3 nm^2, 4.2 nm^2, and 0.5 nm^2, respectively). C), D) Type-A supramolecular trimeric guest of chirality δ within an *R* domain (C, 298 K, $V_s = -1.28$ V, $I = 0.08$ nA) and of chirality λ within an *S* domain (D, 298 K, $V_s = 0.91$ V, $I = 0.09$ nA). E), F) Type-B supramolecular trimeric guest of chirality λ within an *R* domain (E, 298 K, $V_s = 1.13$ V, $I = 0.11$ nA) and of chirality δ within an *S* domain (F, 298 K, $V_s = 1.58$ V, $I = 0.11$ nA). In (C–E), lines indicate the identifiable supramolecular trimer and circles their anchor places to the network. The Ag [1$\bar{1}$0] direction is indicated.

scan time. Two types of propellers, A (yellow) and B (pink), can be identified based on their anchoring points to the host network (Figures 4A and 5C–F). We attribute them to trimeric BPDH supramolecules based on the resemblance of each propeller "blade" to the STM appearance of a single molecule, similar to the trimeric supramolecules observed for bisphenol molecules in a 2D matrix of static molecules[20] and by dicarbonitrile molecules in a hexagonal 2D network.[21] In most cases, the propeller molecules appear dimmer than the network molecules. The high-resolution image in Figure 5C shows burst noise within the pores, which is indicative of rapid molecular motion. This noise, which is absent on the network structure, indicates a position switching of the supramolecule. It can be rationalized by rotation events of the propeller similar to the rotation of the aforementioned supramolecules. We thus tentatively propose that the structures within the pore and surrounding the anchored trimeric propeller are related to transitional positions between rotations of 120°. Both identified supramolecules are chiral and the two enantiomeric propellers are separated in the respective polyporous network domains (Figure 5C–F), a testament to the chirality transfer from the host-network pore to the guest.

In Figure 4D, a closer look at the blue node by AFM reveals that the phenyl moieties of the building blocks exhibit different tilt angles with respect to the surface despite maintaining very similar orientations with respect to the high-symmetry axes. A line appears to join two phenyl moieties of the parallel molecules on the left (indicated by the blue arrow in Figure 4D). Such features do not necessarily indicate chemical bonds or the presence of atoms, but instead were shown to appear due to the bending of the CO on the AFM-tip apex, an effect which can prominently occur for geometrically protruding atoms in close proximity.[22] XPS measurements (Figure 2E) shortly after RT deposition show a decrease in the relative intensity of the O 1s signal attributed to the $^{-}$OH groups, indicating a partial deprotonation of about 30% at RT. Since the polyporous structure is observed following BPDH deposition on an Ag(111) at RT, we relate it to the formation of hydroxamate groups. Here, it should be highlighted that the degrees of freedom of the functional group preclude a systematic modeling of this 2D network: to construct this network, the two fourfold nodes need to be identified. There are six surface amide forms for each surface phenyl hydroxamic acid (Figure 1B) and another four for phenyl hydroxamate. Therefore, the sum of ten possibilities would need to be considered for each of the eight phenyl hydroxamic acid/hydroxamate moieties which compose the blue and red building blocks, adding up to 10^8 combinations. Nevertheless, one can propose an elementary model based on H-bridges to stabilize the network. Here we considered the ten options mentioned above based on the rationale that the small energy difference between the *E*- and *Z*-forms of an isolated molecule in vacuum (Figure S1) could be outweighed by the formation of attractive H-bonding in the network. The possible involvement of Ag adatoms in the supramolecular nodes[23] is unlikely, based on the intermolecular distances. A tentative model is given in Figure 4C: it contains hydroxamate and hydroxamic acid groups in a ratio of 3:5, in accordance with the XPS signals and their configurations labelled as in Figure 1B. The lateral supramolecular interactions in the proposed model consist of (ionic) hydrogen bonding: OH···O=C, NH···O^{-}/NH···O=C, and CH···O^{-}, indicated by orange, green, and yellow ovals, respectively, in Figure 4C. The two highlighted nodes correspond to the blue and red nodes in Figure 4A and are sufficient to model the complete polyporous structure.

Cross-Phase

Coexisting with the polyporous network and occasionally fluently merging with it, we observed domains of a different network comprising fourfold nodes. These nodes have opening angles close to 90°, resembling crosses, leading us to call it the cross-phase. A zoomed-in view of the structure is shown in Figure 6A, whereas an overview can be found in Figure S9A.

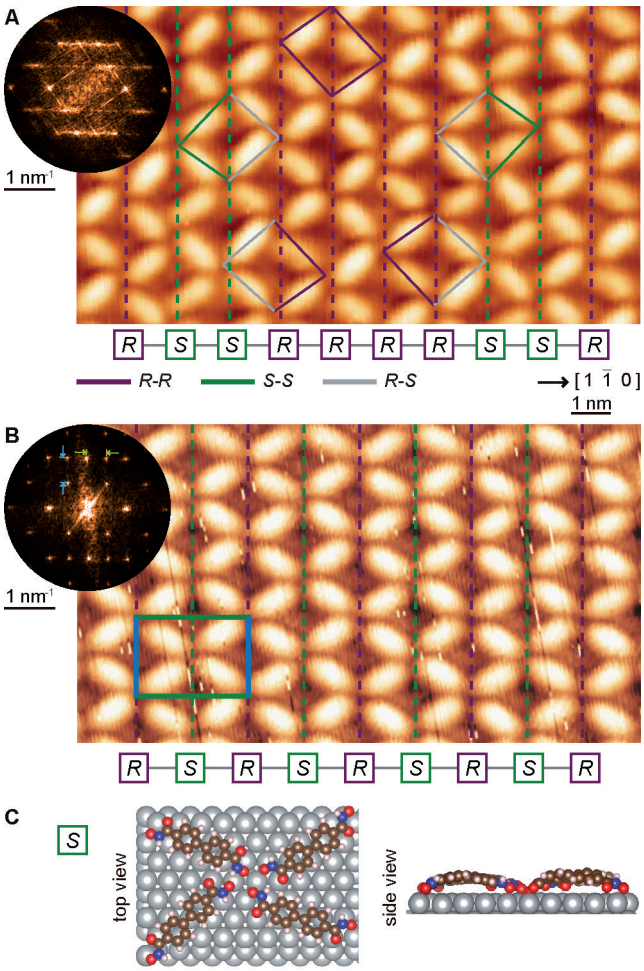

Figure 6. Cross-network of BPDH molecules on Ag(111). A) STM image of the self-assembly of BPDH molecules (140 K, $V_s = 1.06$ V, $I = 0.08$ nA) with *R* (purple) and *S* (green) chiral structures at RT. B) STM image after annealing at 443 K (298 K, $V_s = 1.23$ V, $I = 0.1$ nA). The insets in A and B show the FFT of larger-scale STM data (see also Figure S9). The periodicities of the structure are indicated both in the real- and reciprocal-space representation. C) Top and side view of a simulated *S* node in the ordered racemate. C, O, N, H, and Ag atoms are represented in brown, red, blue, white, and silver color, respectively.

The assembled networks extend to cover atomically flat areas. Examination of the fourfold nodes reveals their chirality, labelled purple and green in Figure 6 to denote *R* and *S*, respectively, analogous to chiral nodes reported in other surface-supramolecular synthons.[24] Both *R* and *S* nodes are found to align along the $[11\bar{2}]$ direction of the Ag surface. Within the 2D networks formed at RT, narrow areas of conglomerates of *R* or *S* node columns (marked by purple and green dashed lines in Figure 6A) are found. The random sequence of *R* and *S* nodes results in a heterogeneity of the pores in the network. Based on the *R*:*S* ratio in the four nodes surrounding each pore, eight possible kinds of chiral rhomboid pores with various dimensions and shapes occur, as shown in Figures 6 and S10. The molecular density of the homochiral structures is about 0.66 molecule nm^{-2}. Since 1D chiral switches are very frequent, one may suggest that the irregular alteration of the *R* and *S* nodes along the $[1\bar{1}0]$ direction of the Ag surface is the signature of 1D randomness (Figure 6A).[25] Indeed, the randomness in these domains is also evident as streaks in the fast Fourier transform (FFT) of the STM micrographs (see inset in Figure 6A and Figure S9B).

However, advancing the control in the expression of this 1D randomness beyond the earlier report,[25] we discovered that after annealing at $\approx$443 K, the randomly distributed *R* and *S* chiral nodes alternate regularly to form an ordered racemic mixture of *RSRS* lines as shown in Figure 6B. This treatment also eliminates the presence of other structures. The *RSRS* cross-structure displays a network of high ordering with fewer defects, as exemplified in larger-scale STM data (Figure S9C), with the corresponding FFT (inset in Figure 6B and Figure S9D) demonstrating sharp spots representing the reciprocal lattice. The rectangular unit cell of the structure (indicated in real-space and reciprocal-space images in Figure 6B) includes one *R* node and one *S* node and has a density of $\approx$0.68 molecules nm^{-2}. Since this structure did not appear on the Au(111) surface, which offers a closely related epitaxial environment, we deduce that it is driven by the chemical interaction of the molecule with the Ag surface.

To rationalize its appearance and the increased order of the reticular superstructure composed by these chiral nodes, we turn our attention to the XPS results in Figure 2E. We consider that the molecules in the 2D network with 1D randomness also contain hydroxamate groups, similar to the polyporous network. The hetero-deprotonation of the molecules drives the 1D random alternation of *R* and *S* nodes. On the contrary, the 2D network with the regular arrangement of racemic nodes consists solely of molecules with hydroxamate groups, based on the low signal of −OH group in XPS measurements after annealing at 373 K (Figure 2E). To propose a molecular model, we performed a DFT simulation of the regular 2D network with a racemic mixture of nodes. Here, a *cis*-isomer with two deprotonated −OH groups is used due to the asymmetric bonding of each molecule: the molecule sides are always involved in one *R* node and one *S* node, whereas a *trans*-isomer would result in homochiral domains. By using the *cis*-isomer, it was also possible to reproduce the observed "long" and "short" intermolecular distances of opposite molecules at the nodes, whereas for the *trans*-isomer, the equal intermolecular distances were found at the nodes. In the simulated structure (Figure 6C), C=O···H−C and N−O···H−N intermolecular hydrogen bonds are found between the two left molecules and C=O···H−C bonding occurs between the two molecules on the right. The side view in Figure 6C reveals that the node is stabilized by a strong interaction with the surface, evidenced by the anchoring of the O atoms, which leads to a bending of the molecular backbone. The result is a unique cross-structure, which appeared only on the silver surface.

Conclusion

In summary, we found that the bioinspired hydroxamic acid linker molecules offer functional groups with great versatility for hydrogen-bonded nodes supported on the noble metals Au and Ag. The related 2D structures exhibited RT stability with densities varying by a factor of almost two between the close-packed and more open phases. Their formation is controlled by a combination of surface coverage and temperature treatment as summarized in Figure S11. We demonstrate that the molecular configuration and the "passive" biphenyl backbone is not a rigid unit but will adapt its adsorption geometry to the different supramolecular assemblies. This finding is important for the design of complex nano-architectures. Interestingly, on the Ag(111) surface, a dynamic adaptation of the supramolecular assemblies is found with the gradual dehydrogenation to hydroxamate. This gives rise to an exceptional polyporous hexagonal framework of unusual complexity, featuring organizational chirality. The degree of dehydrogenation also provides control over the ordering of the chiral nodes in a cross-network: 1D randomness vs. regular racemic 2D networks. Although here, the reactivity of the substrate was used to access the deprotonated state, we note that such states can also be realized in vacuum by employing an electrospray ionization deposition system[26] instead of organic molecular-beam epitaxy. The use of hydroxamic acid as a directing group in surface-supramolecular assemblies can significantly expand the accessible surface tessellations of 2D molecular networks with high potential as templates. To the best of our knowledge, the geometrical tessellation of the polyporous framework was not achieved by molecular architectonics yet. We anticipate that the polyporous network can provide a template with considerable size selectivity for, for example, nanoparticles, whereas the chirality of the pores in these networks can lead to the chiral recognition of larger guest molecules. Indeed, the larger pores are shown to promote the formation of enantiospecific trimeric supramolecular guests. This is another demonstration of a dynamic adaptation of the supramolecular building block: from the fourfold node assembly of the host to the threefold node assembly of the guest, guided by the spatial confinement and the host-grid arrangement.

Acknowledgements

We acknowledge funding by the Postdoctoral Council of China (2015 International Postdoctoral Exchange Fellowship Program, C.J.), the China Scholarship Council (B.Z., L.J.), the International Max Planck Research School of Advanced Photon Science (S.S.), the European Union's Horizon 2020 research and innovation programme (grant agreement no. 664878), the European Research Council Consolidator Grant NanoSurfs (no. 615233), and the Deutsche Forschungsgemeinschaft (Excellence Cluster Munich-Centre for Advanced Photonics and Heisenberg professorship, W.A.). Computations were performed on the shared Hierarchical Academic Research Computing Network (SHARCNET) and the Cedar, Graham, and Niagara clusters of Compute/Calcul Canada.

Conflict of interest

The authors declare no conflict of interest.

Keywords: atomic force microscopy · host–guest systems · hydroxamic acid · scanning tunneling microscopy · two-dimensional nanostructures

How to cite: *Angew. Chem. Int. Ed.* **2019**, *58*, 18948–18956
Angew. Chem. **2019**, *131*, 18948–19132

[1] a) X. Bouju, C. Mattioli, G. Franc, A. Pujol, A. Gourdon, *Chem. Rev.* **2017**, *117*, 1407–1444; b) D. P. Goronzy, M. Ebrahimi, F. Rosei, Arramel, Y. Fang, S. De Feyter, S. L. Tait, C. Wang, P. H. Beton, A. T. S. Wee, P. S. Weiss, D. F. Perepichka, *ACS Nano* **2018**, *12*, 7445–7481; c) J. A. A. W. Elemans, S. B. Lei, S. De Feyter, *Angew. Chem. Int. Ed.* **2009**, *48*, 7298–7332; *Angew. Chem.* **2009**, *121*, 7434–7469; d) J. V. Barth, *Annu. Rev. Phys. Chem.* **2007**, *58*, 375–407; e) J. V. Barth, G. Costantini, K. Kern, *Nature* **2005**, *437*, 671–679.

[2] a) K. S. Mali, N. Pearce, S. De Feyter, N. R. Champness, *Chem. Soc. Rev.* **2017**, *46*, 2520–2542; b) L. Sosa-Vargas, E. Kim, A. J. Attias, *Mater. Horiz.* **2017**, *4*, 570–583.

[3] J. Shang, Y. Wang, M. Chen, J. Dai, X. Zhou, J. Kuttner, G. Hilt, X. Shao, J. M. Gottfried, K. Wu, *Nat. Chem.* **2015**, *7*, 389–393.

[4] F. Cheng, X.-J. Wu, Z. Hu, X. Lu, Z. Ding, Y. Shao, H. Xu, W. Ji, J. Wu, K. P. Loh, *Nat. Commun.* **2018**, *9*, 4871.

[5] a) D. Écija, J. I. Urgel, A. P. Seitsonen, W. Auwärter, J. V. Barth, *Acc. Chem. Res.* **2018**, *51*, 365–375; b) D. Écija, J. I. Urgel, A. C. Papageorgiou, S. Joshi, W. Auwärter, A. P. Seitsonen, S. Klyatskaya, M. Ruben, S. Fischer, S. Vijayaraghavan, J. Reichert, J. V. Barth, *Proc. Natl. Acad. Sci. USA* **2013**, *110*, 6678–6681; c) J. I. Urgel, D. Écija, G. Lyu, R. Zhang, C.-A. Palma, W. Auwärter, N. Lin, J. V. Barth, *Nat. Chem.* **2016**, *8*, 657–662.

[6] a) M. Manal, M. J. N. Chandrasekar, J. Gomathi Priya, M. J. Nanjan, *Bioorg. Chem.* **2016**, *67*, 18–42; b) D. Weigt, C. Hopf, G. Médard, *Clin. Epigenet.* **2016**, *8*, 76; c) R. Kakkar in *Hydroxamic Acids: A Unique Family of Chemicals with Multiple Biological Activities* (Ed.: S. P. Gupta), Springer Berlin Heidelberg, Berlin, **2013**, pp. 19–53.

[7] a) B. Rudshteyn, C. F. A. Negre, R. S. Oliboni, A. Monti, J. Chen, R. H. Crabtree, L. G. C. Rego, V. S. Batista, *J. Phys. Chem. C* **2017**, *121*, 11985–11990; b) T. Higashino, Y. Kurumisawa, N. Cai, Y. Fujimori, Y. Tsuji, S. Nimura, D. M. Packwood, J. Park, H. Imahori, *ChemSusChem* **2017**, *10*, 3347–3351; c) S. H. Aung, Y. Hao, T. Z. Oo, G. Boschloo, *ACS Omega* **2017**, *2*, 1820–1825.

[8] a) W. Tieu, T. Lifa, A. Katsifis, R. Codd, *Inorg. Chem.* **2017**, *56*, 3719–3728; b) J. P. Folkers, C. B. Gorman, P. E. Laibinis, S. Buchholz, G. M. Whitesides, R. G. Nuzzo, *Langmuir* **1995**, *11*, 813–824.

[9] a) D. Kaur, R. Kohli, *Struct. Chem.* **2011**, *23*, 161–173; b) D. Kaur, R. Kohli, *Int. J. Quantum Chem.* **2011**, *111*, 2931–2943.

[10] R. Kakkar, R. Grover, P. Chadha, *Org. Biomol. Chem.* **2003**, *1*, 2200–2206.

[11] B. Schuler, W. Liu, A. Tkatchenko, N. Moll, G. Meyer, A. Mistry, D. Fox, L. Gross, *Phys. Rev. Lett.* **2013**, *111*, 106103.

[12] a) S. Kawai, S. Nakatsuka, T. Hatakeyama, R. Pawlak, T. Meier, J. Tracey, E. Meyer, A. S. Foster, *Sci. Adv.* **2018**, *4*, eaar7181; b) C. Krull, M. Castelli, P. Hapala, D. Kumar, A. Tadich, M. Capsoni, M. T. Edmonds, J. Hellerstedt, S. A. Burke, P. Jelinek, A. Schiffrin, *Nat. Commun.* **2018**, *9*, 3211; c) L. Gross, F. Mohn, N. Moll, G. Meyer, R. Ebel, W. M. Abdel-Mageed, M. Jaspars, *Nat. Chem.* **2010**, *2*, 821–825; d) X. Zhang, N. Xue, C. Li, N. Li, H. Wang, N. Kocić, S. Beniwal, K. Palotás, R. Li, Q. Xue, S. Maier, S. Hou, Y. Wang, *ACS Nano* **2019**, *13*, 1385–1393.

[13] a) L. Feng, T. Wang, Z. Tao, J. Huang, G. Li, Q. Xu, S. L. Tait, J. Zhu, *ACS Nano* **2019**, *13*, 10603–10611; b) S. C. Oh, J. A. Lloyd, S. Fischer, Ö. Saglam, A. C. Papageorgiou, K. Diller, D. A. Duncan, F. Klappenberger, F. Allegretti, J. Reichert, J. V. Barth, *Chem. Commun.* **2018**, *54*, 12495–12498; c) P. S. Deimel, K. Stoiber, L. Jiang, J. A. Lloyd, S. C. Oh, S. Fischer, Ö. Sağlam, H. Schlichting, A. C. Papageorgiou, J. V. Barth, F. Allegretti, J. Reichert, *J. Phys. Chem. C* **2019**, *123*, 1354–1361.

[14] a) N. Zhu, T. Osada, T. Komeda, *Surf. Sci.* **2007**, *601*, 1789–1794; b) W. D. Xiao, Y. H. Jiang, K. Ait-Mansour, P. Ruffieux, H. J. Gao, R. Fasel, *J. Phys. Chem. C* **2010**, *114*, 6646–6649; c) T. Schmitt, L. Hammer, M. A. Schneider, *J. Phys. Chem. C* **2016**, *120*, 1043–1048; d) D. Schwarz, R. van Gastel, H. J. W. Zandvliet, B. Poelsema, *J. Phys. Chem. C* **2013**, *117*, 1020–1029.

[15] B. Quiroga Argañaraz, L. J. Cristina, L. M. Rodríguez, A. Cossaro, A. Verdini, L. Floreano, J. D. Fuhr, J. E. Gayone, H. Ascolani, *Phys. Chem. Chem. Phys.* **2018**, *20*, 4329–4339.

[16] a) A. C. Papageorgiou, S. Fischer, J. Reichert, K. Diller, F. Blobner, F. Klappenberger, F. Allegretti, A. P. Seitsonen, J. V. Barth, *ACS Nano* **2012**, *6*, 2477–2486; b) R. E. A. Kelly, L. N. Kantorovich, *Surf. Sci.* **2005**, *589*, 139–152; c) R. E. A. Kelly, L. N. Kantorovich, *J. Phys. Chem. B* **2006**, *110*, 2249–2255.

[17] a) J. V. Barth, J. Weckesser, G. Trimarchi, M. Vladimirova, A. D. Vita, C. Z. Cai, H. Brune, P. Gunter, K. Kern, *J. Am. Chem. Soc.* **2002**, *124*, 7991–8000; b) J. Weckesser, A. De Vita, J. V. Barth, C. Cai, K. Kern, *Phys. Rev. Lett.* **2001**, *87*, 096101; c) C. Lin, E. Durant, M. Persson, M. Rossi, T. Kumagai, *J. Phys. Chem. Lett.* **2019**, *10*, 645–649.

[18] S. M. Barlow, R. Raval, *Surf. Sci. Rep.* **2003**, *50*, 201–341.

[19] J. Teyssandier, S. D. Feyter, K. S. Mali, *Chem. Commun.* **2016**, *52*, 11465–11487.

[20] J. A. Lloyd, A. C. Papageorgiou, S. Fischer, S. C. Oh, Ö. Sağlam, K. Diller, D. A. Duncan, F. Allegretti, F. Klappenberger, M. Stöhr, R. J. Maurer, K. Reuter, J. Reichert, J. V. Barth, *Nano Lett.* **2016**, *16*, 1884–1889.

[21] a) D. Kühne, F. Klappenberger, W. Krenner, S. Klyatskaya, M. Ruben, J. V. Barth, *Proc. Natl. Acad. Sci. USA* **2010**, *107*, 21332–21336; b) C. A. Palma, J. Bjork, F. Klappenberger, E. Arras, D. Kuhne, S. Stafstrom, J. V. Barth, *Nat. Commun.* **2015**, *6*, 6210.

[22] P. Hapala, G. Kichin, C. Wagner, F. S. Tautz, R. Temirov, P. Jelínek, *Phys. Rev. B* **2014**, *90*, 085421.

[23] a) A. C. Papageorgiou, J. Li, S. C. Oh, B. Zhang, Ö. Sağlam, Y. Guo, J. Reichert, A. B. Marco, D. Cortizo-Lacalle, A. Mateo-Alonso, J. V. Barth, *Nanoscale* **2018**, *10*, 9561–9568; b) F.

De Marchi, G. Galeotti, M. Simenas, E. E. Tornau, A. Pezzella, J. MacLeod, M. Ebrahimi, F. Rosei, *Nanoscale* **2018**, *10*, 16721 – 16729.

[24] a) S. Stepanow, N. Lin, D. Payer, U. Schlickum, F. Klappenberger, G. Zoppellaro, M. Ruben, H. Brune, J. V. Barth, K. Kern, *Angew. Chem. Int. Ed.* **2007**, *46*, 710 – 713; *Angew. Chem.* **2007**, *119*, 724 – 727; b) P. Messina, A. Dmitriev, N. Lin, H. Spillmann, M. Abel, J. V. Barth, K. Kern, *J. Am. Chem. Soc.* **2002**, *124*, 14000 – 14001.

[25] Y.-Q. Zhang, T. Lin, B. Cirera, R. Hellwig, C.-A. Palma, Z. Chen, M. Ruben, J. V. Barth, F. Klappenberger, *Angew. Chem. Int. Ed.* **2017**, *56*, 7797 – 7802; *Angew. Chem.* **2017**, *129*, 7905 – 7910.

[26] C. Méthivier, V. Humblot, C.-M. Pradier, *J. Phys. Chem. C* **2016**, *120*, 27364 – 27368.

Manuscript received: September 25, 2019
Accepted manuscript online: October 31, 2019
Version of record online: November 27, 2019

